J Neurophysiol 120: 893–909, 2018.
First published May 9, 2018; doi:10.1152/jn.00643.2017.

RESEARCH ARTICLE | *Control of Movement*

Neck muscle spindle noise biases reaches in a multisensory integration task

Parisa Abedi Khoozani[1,2] and Gunnar Blohm[1,2,3]

[1]*Centre for Neuroscience Studies, Queen's University, Kingston, Ontario, Canada;* [2]*Canadian Action and Perception Network, Toronto, Ontario, Canada; and* [3]*Association for Canadian Neuroinformatics and Computational Neuroscience, Kingston, Ontario, Canada*

Submitted 31 August 2017; accepted in final form 25 April 2018

Abedi Khoozani P, Blohm G. Neck muscle spindle noise biases reaches in a multisensory integration task. *J Neurophysiol* 120: 893–909, 2018. First published May 9, 2018; doi:10.1152/jn.00643.2017.—Reference frame transformations (RFTs) are crucial components of sensorimotor transformations in the brain. Stochasticity in RFTs has been suggested to add noise to the transformed signal due to variability in transformation parameter estimates (e.g., angle) as well as the stochastic nature of computations in spiking networks of neurons. Here, we varied the RFT angle together with the associated variability and evaluated the behavioral impact in a reaching task that required variability-dependent visual-proprioceptive multisensory integration. Crucially, reaches were performed with the head either straight or rolled 30° to either shoulder, and we also applied neck loads of 0 or 1.8 kg (left or right) in a 3 × 3 design, resulting in different combinations of estimated head roll angle magnitude and variance required in RFTs. A novel three-dimensional stochastic model of multisensory integration across reference frames was fitted to the data and captured our main behavioral findings: *1*) neck load biased head angle estimation across all head roll orientations, resulting in systematic shifts in reach errors; *2*) increased neck muscle tone led to increased reach variability due to signal-dependent noise; and *3*) both head roll and neck load created larger angular errors in reaches to visual targets away from the body compared with reaches toward the body. These results show that noise in muscle spindles and stochasticity in general have a tangible effect on RFTs underlying reach planning. Since RFTs are omnipresent in the brain, our results could have implications for processes as diverse as motor control, decision making, posture/balance control, and perception.

NEW & NOTEWORTHY We show that increasing neck muscle tone systematically biases reach movements. A novel three-dimensional multisensory integration across reference frames model captures the data well and provides evidence that the brain must have online knowledge of full-body geometry together with the associated variability to plan reach movements accurately.

body geometry; computational modeling; multisensory integration; muscle spindle noise; stochastic reference frame transformation

INTRODUCTION

Different sensory and motor signals are encoded in different coordinates in the brain, e.g., early vision in eye/gaze-centered, primary arm proprioception in shoulder-centered. Conversions between reference frames are vital to transform signals into reference frames that are appropriate for processes as diverse as motor control, decision making, posture/balance control, and perception (Blohm and Crawford 2007; Buneo et al. 2002; Flanders et al. 1992; Knudsen et al. 1987; Soechting and Flanders 1992; Vetter et al. 1999). Previous studies have suggested that reference frame transformations (RFTs) should be regarded as stochastic processes that modulate the reliability of transformed signals (Alikhanian et al. 2015; Burns and Blohm 2010; Burns et al. 2011; Schlicht and Schrater 2007). Furthermore, several studies proposed that humans flexibly select the coordinates that minimize the effect of stochasticity (Sober and Sabes 2005). Cue reliability-based multisensory integration studies have shown that stochastic RFTs affect human behavior (Burns and Blohm 2010; Burns et al. 2011; Schlicht and Schrater 2007); however, the sources of stochasticity in RFTs as well as the underlying mechanisms of how RFTs affect transformed signals remain unclear.

To perform RFTs accurately, the brain must have an estimate of three-dimensional (3D) body articulation (Blohm and Crawford 2007), i.e., an internal estimate of different body parts with regard to each other (such as eye relative to head translation) as well as an estimate of joint angles (such as head/eye orientations). Whereas the former is likely learned and does not change, the latter could stem from at least two sources, noisy afferent sensory signals (proprioception) and efferent copies of motor commands. Both signals are inherently variable due to the uncertainty of sensory reading and the variability of neuronal spiking (Poisson noise). Several studies have suggested that varying body articulation, e.g., the head roll (HR) angle, increases the behavioral variability due to signal-dependent sensory and neural noise affecting the RFT (Alikhanian et al. 2015; Burns and Blohm 2010; Burns et al. 2011; Schlicht and Schrater 2007). Signal-dependent sensory noise can arise from variability in the muscle spindle activity, the vestibular system, or both (Cordo et al. 2002; Faisal et al. 2008; Lechner-Steinleitner 1978; Sadeghi et al. 2007; Scott and Loeb 1994). Thus larger joint angle estimates are accompanied by higher uncertainty (Blohm and Crawford 2007; Van Beuzekom and Van Gisbergen 2000; Wade and Curthoys 1997), which results in an increased trial-to-trial variability in the RFT.

The effect of stochastic RFTs on the reliability of transformed signals has been studied using a multisensory integration task. Multisensory integration combines different sources of sensory information to create the best possible estimate of

Address for reprint requests and other correspondence: G. Blohm, Queen's Univ., Botterell Hall, 18 Stuart St., Kingston, ON, Canada K7L3N6 (e-mail: gunnar.blohm@queensu.ca).

the state of our body within the environment in a way that is generally well-captured by Bayes-optimal integration (Atkins et al. 2001; Ernst and Banks 2002; Ernst and Bülthoff 2004; Kersten et al. 2004; Knill and Pouget 2004; Körding and Wolpert 2006; Landy et al. 1995; Landy and Kojima 2001; Stein and Meredith 1993; Stein and Stanford 2008). For instance, both visual and proprioceptive information can be combined in a reliability-weighted fashion to estimate hand position. It is believed (weak fusion hypothesis, Clark and Yuille 1990) that before integration, any signals must first be converted into a common coordinate system; this requires a (stochastic) RFT. Within this framework, the reliability of the transformed signal is affected by stochasticity in RFTs (Alikhanian et al. 2015), thus modulating the multisensory integration weights (Burns and Blohm 2010; Burns et al. 2011). It is not clear, however, what the consequences of varying the noise in the parameters involved in RFT processes are. More specifically, it is not clear how varying multisensory weights due to stochastic RFTs affects reaching movements to visual targets.

Here, we deployed a modified version of the standard visual-proprioceptive integration-based reaching task (Sober and Sabes 2003, 2005; van Beers et al. 1999) to investigate systematically the behavioral consequences of biases and variability in sensory estimates used for stochastic RFTs. We asked human participants to perform a center-out reaching task while the seen and actual hand positions were dissociated. In addition, reaches were performed with the head either straight or rolled 30° to either shoulder, and we also applied neck loads (NLs) of 0 or 1.8 kg (left or right) in a 3 × 3 design. Our results demonstrate that applying the NL increased the variability of reach movements and biased the reaching behavior toward the applied load in all HR orientations. Our prediction was that these effects on reaching behavior can be explained by a change in multisensory integration weights due to stochastic RFTs, which consequently enabled us to quantify the relative contribution of neck muscle spindles to the estimation of HR angle. To test this hypothesis, we implemented a novel 3D stochastic model of multisensory integration across reference frames. Our model was able to capture the pattern of behavioral data well and allowed us to make two main conclusions: the effect of NL on reaching behavior can be explained by changes in multisensory weights due to stochastic RFTs and the source of this stochasticity in RFTs is signal-dependent noise.

MATERIALS AND METHODS

Participants

Nine healthy humans (eight men) between 20 and 35 yr of age with normal or corrected-to-normal vision participated in our reaching task. They performed their reaching with their dominant, right hand. Experimental conditions were approved by the Queen's University General Research Ethics Board, and all of the participants gave their written consent. Monetary compensation was provided for participating in the experiment ($10/h).

Apparatus

A virtual reality robotic setup (KINARM end-point robot; BKIN Technologies) was used for performing the center-out reaching task. Participants stood in front of the robot while positioning their head by resting the forehead on the robot in front of the screen and their chin on a chinrest. Participants grasped a vertical handle attached to the robotic arm to reach to the viewed target on the mirrored surface. The vision of participants' hand was occluded using an opaque board, and eye movements were tracked using embedded technology (EyeLink 1000; SR Research). A pulley system and a helmet were used for measuring the HR and NL (see Fig. 1, *A* and *C*).

Task Design

Participants stood in front of the robot and grasped the handle. At the beginning of each trial, participants were instructed to position their hand on the start position (cross) in the center of the display field. The robotic arm moved the hand toward the center and released it when the hand was within 3 cm of the central cross; a red dot representing hand position appeared at this point. After the participant positioned the hand correctly on the cross, one of the eight targets, distributed evenly on a circle with radius 10 cm, appeared. Participants were instructed to move through the target quickly and accurately while keeping their gaze fixated on the center cross. Once the participant's hand begun to move (85 mm/s velocity threshold), the hand cursor disappeared. If they reached the target in <750 ms, the trial was successful and participants would hear a success beep, otherwise a failure beep was played indicating that the trial had been aborted and would have to be repeated. At the end of each trial, the center cross disappeared and participants had to wait 500 ms to start the next trial. The next trial started with the reappearance of the center cross and the movement of the robotic arm driving the participant's hand to the start position. This was to ensure that participants did not have visual feedback of the performance of their previous trial.

There were several different conditions in our experiment. The hand was physically shifted randomly either up/down or left/right with respect to the visual feedback of the hand. For example, participants would align their hand cursor to the center cross while their actual hand position was 2.5 cm left of the cross. This discrepancy was introduced to enable us to measure the relative weighting of vision and proprioception in the multisensory integration process, similar to the logic employed in Sober and Sabes (2003, 2005) and Burns and Blohm (2010). In addition, the reaching movements were performed while the participants either kept their head straight or

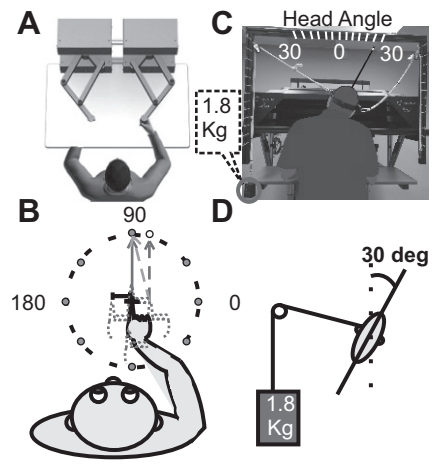

Fig. 1. Apparatus. *A*: KINARM end-point robot arrangement [from http://www.bkintechnologies.com/ with permission from BKIN Technologies Ltd., Kingston, Ontario, Canada]. *B*: visual targets were distributed evenly on a 10-cm-radius circle. The hand was shifted 2.5 cm either vertically or horizontally while the visual indicator stayed at the center. *C*: picture of the pulley system for measuring the head roll and loading the neck; here, the participant had 30° (30 deg) clockwise head roll and neck load on the left side. *D*: schematic of the condition represented in *C*. The attached indicator on the helmet was used to measure the head angle.

rolled their head 30° toward each shoulder and while an NL (0 or 1.8 kg) was applied to the left or right side (the value of the weight was chosen to stimulate the same force as a 30° HR on neck muscles). Combinations of different HR and NL conditions are shown in Fig. 2. We hypothesized that altering HR and neck muscle force would create a conflict for HR estimation as well as changing the signal-dependent noise, which will affect the weights of multisensory integration. Participants completed 640 trials (5 hand positions × 8 targets × 16 repetitions) for each of the 9 combinations of HR/NL, for a total of 5,760 trials (640 × 9) in 6 1-h sessions. To avoid any biases due to a specific order of experiment conditions, we employed Latin squares method to counterbalance among different experimental conditions (Jacobson and Matthews 1996).

Data Analysis

Hand and eye movement were captured with sampling rates of 1,000 and 500 Hz, respectively. MATLAB software was used for offline analysis: a low-pass filter (autoregressive forward-backward filter, cutoff frequency = 50 Hz) was used to smooth the acquired data. First and second derivative of hand position data were calculated (using a central difference algorithm) to obtain hand velocity and acceleration. Trials in which participants moved their eyes after the visual target is displayed or moved their hand in a predictive direction except the target direction were removed (3% of overall trials). The time span from when participants started to move until their hand crossed a 9-cm circle is defined as the initial movement duration. Movements were typically straight and had very little curvature; thus movement angle was derived through regression of data points acquired throughout the initial movement duration. Since the visual and proprioceptive hand position were dissociated, we defined visual movement as the movement obtained when subtracting visual hand from target information (darker gray arrow, Fig. 1*B*) and proprioceptive movement as the movement direction obtained when subtracting proprioceptive hand position from the visual target information (lighter gray arrow, Fig. 1*B*). Subtracting predicted visual (proprioceptive) movement from the measured movement angle yielded the directional visual (proprioceptive) movement errors, which we used for our analysis. We then used an analytical model to capture the pattern of movement errors measured across conditions and targets (see *Model Description* below).

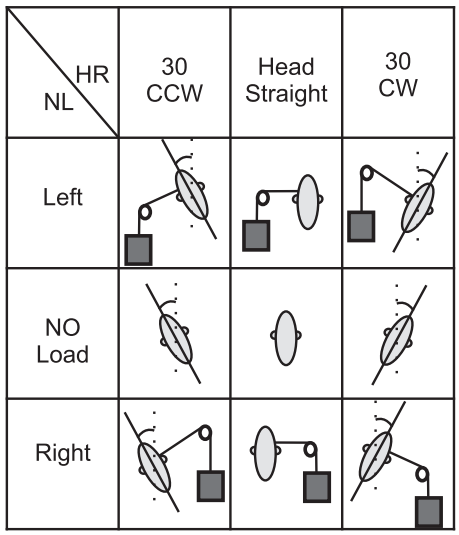

Fig. 2. Experimental conditions. Participants performed the reaching task under 9 different combinations of head roll (HR) and neck load (NL) conditions during our experiment. CCW, counterclockwise; CW, clockwise.

Statistical Analysis

An *n*-way repeated-measures ANOVA was used to assess the statistical differences (MATLAB 2013a, anovan.m), and post hoc analysis using the Bonferroni criterion (MATLAB 2013a, multcompare.m) was performed to assess the interaction between different parameters. A paired *t*-test (MATLAB 2013a, ttest.m) was used to assess the statistical significance in reach error variability for different HR and NL conditions. In all of the statistical analysis, $P < 0.001$ was considered as the criterion for statistical significance.

Model Description

The goal of our model was to understand which intrinsic and extrinsic variables were required to perform the RFTs accurately and, more importantly, how variation of such variables affects human movement behavior. To understand the effect of RFTs on reach planning, we first explain the required steps in our model to plan a reach movement. Sober and Sabes (2003) proposed a two-step model for planning a reach movement in which first a movement plan is calculated by subtracting the hand position from the target position. Then, this movement plan transformed to a desired change in arm angles through performing inverse kinematics. We extended previous models (Burns and Blohm 2010; Sober and Sabes 2003) that considered two steps for planning a reach movement: *1*) calculating the movement plan and *2*) generating the motor command. Several neurophysiology studies suggested that the movement plan is coded in visual (retinal) coordinates (Andersen and Buneo 2002; Batista et al. 1999), whereas motor commands are coded in joint coordinates (Crawford et al. 2004). Following the same logic, in our model, the two steps were performed in two different coordinates, respectively: visual and proprioceptive coordinates. Visual information of hand and target positions were coded as retinal information in gaze-centered coordinates, $X_h = (x_{1,h}, x_{2,h})$ and $X_t = (x_{1,t}, x_{2,t})$, respectively (Fig. 3, *left*), whereas the proprioceptive information of initial hand position was coded as joint angles in shoulder-centered coordinates, $(\theta_{1,h}, \theta_{2,h})$ (Fig. 3, *right*).

Reference Frame Transformation

To transform information between the visual and proprioceptive coordinates accurately, the full-body geometry must be taken into account (Blohm and Crawford 2007). This is specifically important when the head is not straight, i.e., rotating the head results in shifts of centers of rotation of the eye, head, and shoulder relative to each other (Henriques and Crawford 2002; Henriques et al. 2003). To capture this, we performed a series of rotations (R) and translations (T), formulated in *Eqs. 1* and *2*, respectively.

$$X_{\text{rotated}} = \mathrm{R} X_{\text{original}} \quad (1)$$

Where $\mathrm{R} = \begin{bmatrix} \cos\theta & \sin\theta \\ -\sin\theta & \cos\theta \end{bmatrix}$, $\theta > 0$ holds for clockwise rotations.

$$X_{\text{translated}} = X_{\text{original}} + \mathrm{T} \quad (2)$$

In the following section, we explain the required steps to transform hand position from retinal-centered to shoulder-centered coordinates. The transformation from shoulder-centered to retinal-centered is a similar process only in the reverse order.

Retinal-to-Shoulder Transformation

As is depicted in Fig. 3, to transform retinal-coded information into joint-coded information, the theoretically required sequential transformations can be done by first transforming retinal to head coordinates, then from head to shoulder, and finally from shoulder to joint coordinates (note that this is likely different from how the brain is performing this transformation).

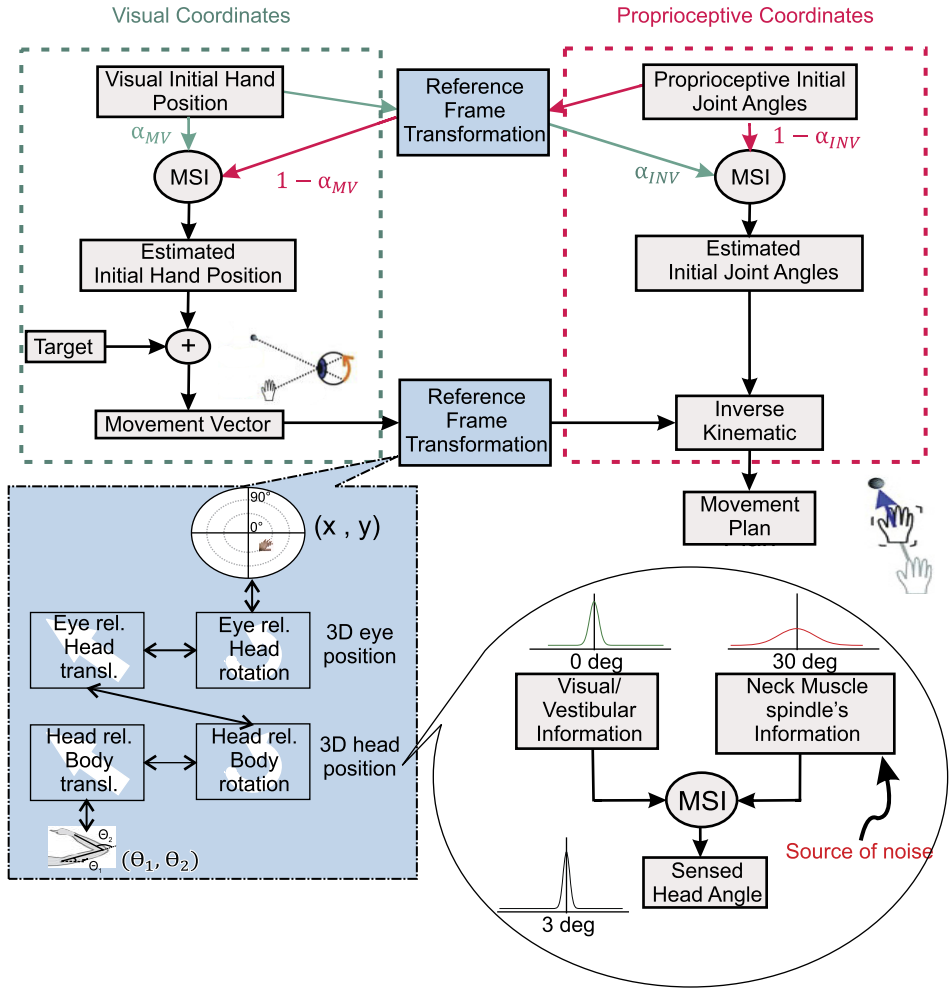

Fig. 3. Model schematic. To perform the reach movement successfully, initial hand position (IHP) is calculated in both visual and proprioceptive coordinates. In visual coordinates, IHP is computed by transforming proprioceptive information into visual coordinates. Visual and transformed proprioceptive information are weighted and combined based on Bayesian theory. Movement vector is calculated by comparing the estimated IHP and target positions. The same process takes place in proprioceptive coordinates to generate a proprioceptive IHP estimate. With the use of inverse kinematics, the transformed movement vector and IHP can be combined to calculate the movement plan based on the required changes in joint angles. The blue box represents the reference frame transformation (RFT) process. RFTs are performed by considering eye and head orientation as well as the translations (transl.) between rotation centers of the body. Head orientation is estimated by combining visual/vestibular and neck muscle spindle information using Bayesian statistics (see MATERIALS AND METHODS for details). α_{INV}, multisensory weight for visual information in proprioceptive coordinates; α_{MV}, multisensory integration (MSI) weight for visual information in visual coordinates; θ_1 and θ_2, joint angles in shoulder-centered coordinates; 3D, 3-dimensional; deg, degrees; rel., relative to.

Retinal-to-head.

$$X^{v}_{h,eye} = R_{eye} X^{v}_{h,retinal} \quad (3)$$

$$X^{v}_{h,head} = R_{head}(X^{v}_{h,eye} + T_{eye\text{-}head}) \quad (4)$$

R_{eye} and R_{head} are rotations based on eye angle and head angle, respectively, and $T_{eye\text{-}head}$ is the translation between eye and head, which is the distance between the center of two eyes (eye-centered coordinate) and the joint of head and neck (head-centered coordinate). $X^{v}_{h,eye}$ is the visual information of hand position in eye-centered coordinate: subscript "h" represents information related to the hand position, and the following subscript represents the related coordinate at that step. In addition, we deployed superscripts "v" or "p" to dissociate if the information is originally provided by vision or proprioception, respectively. All of the following parameters have the same pattern.

Head-to-shoulder.

$$X^{v}_{h,shoulder} = X^{v}_{h,head} + T_{head\text{-}shoulder} \quad (5)$$

Since the body was upright, a translation is sufficient to perform the transformation between the shoulder and head. In our setup, the shoulder was located downward and to the right of the head.

Shoulder-to-joint.

$$\theta^{v}_{h,joint} = A(x^{0}) X^{v}_{h,shoulder} \quad (6)$$

$A(x^0)$ is the forward kinematic matrix and has the same form as *Eq. 7* by Burns and Blohm (2010), since our experimental configuration is the same. To transform the information from joint angle coordinates to retinal coordinates, the same procedure can be performed only in the reverse order [since we used the same configuration as Burns and Blohm (2010), both forward and inverse kinematic matrices have the same format].

In addition to the full-body geometry, we considered the noise of transformation in our model. Similar to Burns and Blohm (2010), we have two noise components resulting from the transformation: fixed-transformation noise (σ^2_{FT}) to simulate the fact that any transformation has a cost (Sober and Sabes 2005) and variable transformation noise (σ^2_{VT}) to simulate the different head orientations and NL conditions of our experiment (this is the same as the variability in the estimated head angle).

Estimating Head Angle

As mentioned in the previous section, participants performed reaching with different HR and NL conditions. Therefore, our model must include a head angle estimation component as a crucial part of the RFT processes. Previous studies showed that humans combine visual, vestibular, and neck proprioceptive information for estimating head orientation, similar to a Bayesian optimal observer (Alberts et al. 2016; Clemens et al. 2011; Mergner et al. 1983, 1991, 1997). For instance, Mergner et al. (1991) demonstrated that the stimulation of neck muscles by rotating the trunk on a fixed head caused a sensation of head rotation and also increased the uncertainty of head position estimation. In addition, two studies carried out in Medendorp's group (Alberts et al. 2016; Clemens et al. 2011) demonstrated that the noise in both vestibular and proprioceptive information should be considered signal-dependent. Thus, following the same rationale, we in-

cluded NL in our experimental condition with the goal of investigating the contribution of the mentioned sources of information for estimating the head angle. Assuming that each source of information has a Gaussian distribution, the head angle signal has a Gaussian distribution as well, and its mean and variance can be estimated as follows:

$$\delta^2_{HA} = \frac{\delta^2_{V/V} \times \delta^2_{NM}}{\delta^2_{V/V} + \delta^2_{NM}} \quad (7)$$

$$\mu_{HA} = \frac{\delta^2_{HA}}{\delta^2_{V/V}} \times \mu_{V/V} + \frac{\delta^2_{HA}}{\delta^2_{NM}} \times \mu_{NM}, \quad (8)$$

in which δ^2_{HA}, $\delta^2_{V/V}$, and δ^2_{NM} are associated variability in head angle estimation, visual/vestibular information, and neck muscle information, respectively, and μ_{HA}, $\mu_{V/V}$, and μ_{NM} are the associated means in the same order. Therefore, we also were able to extract the relative visual/vestibular vs. neck muscle contribution in estimating head angle ($C = \frac{\delta^2_{NM}}{\delta^2_{V/V}}$).

As mentioned earlier, one of the key features of our model is including signal-dependent noise in our RFTs: higher signal value (due to HR) results in higher variability of both vestibular and neck muscle spindle signals. In addition, applying the NL increases the force on the neck muscle, which results in higher variability of the neck muscle spindle signal. In the conditions of applying the NL while the head is not straight, the two forces on the neck muscle are combined to drive the predicted neck muscle force. Therefore, we differentiated the variability for the head straight and no load condition from the other HR and NL conditions. Similar to Vingerhoets et al. (2009), we used a linear model to explain the increase in variability due to increase in the signal value:

$$\delta^2_{V/V} = \delta^2_{V/V,h0} + \text{head roll} \times \delta^2_{V/V,h\neq 0} \quad (9)$$

$$\delta^2_{NM} = \delta^2_{NM,h0} + \text{muscle force from } (\text{HR \& NL}) \times \delta^2_{NM,h\neq 0}, \quad (10)$$

in which $\delta^2_{V/V,h0}$ and $\delta^2_{NM,h0}$ are visual/vestibular and neck muscle variability for head straight condition and $\delta^2_{V/V,h\neq 0}$ and $\delta^2_{NM,h\neq 0}$ are the ones for other experimental conditions. This will result in having $\mu_{HA,h0}$ and $\mu_{HA,h\neq 0}$. At the final step, the required head angle for the transformation (θ_{HA}) is derived by scaling the estimated head angle (μ_{HA}, obtained by sampling from the above Gaussian distribution) by a gain factor, β: $\theta_{HA} = \beta \times \mu_{HA}$.

Multisensory Integration

To estimate the initial hand position (IHP), visual (V) and proprioceptive (P) information are combined using multisensory integration principles. In our model, the multisensory integration is happening twice: once in visual coordinates (coded in Euclidean) to calculate the movement vector (MV) and once in proprioceptive coordinates (coded in joint angles) to generate the motor command using inverse kinematics (INV). We assumed that each piece of information has a Gaussian distribution (before and after RFTs), and, therefore, using multivariate Gaussian statistics, the mean and covariance of the combined IHP estimated from vision (V) and proprioception (P) in each coordinate can be written as:

$$\sum_{IHP} = \left(\sum_P^{-1} + \sum_V^{-1}\right)^{-1} \quad (11)$$

$$\mu_{IHP} = \sum_{IHP}\sum_P^{-1}\mu_P + \sum_{IHP}\sum_V^{-1}\mu_V, \quad (12)$$

where $\sum_{IHP}$ is the covariance matrix of IHP and $\sum_V$ and $\sum_P$ are covariance matrices of visual and proprioceptive information, respectively. Similarly, μ_{IHP}, μ_P, and μ_V are the mean values (in the vector format) for IHP, visual, and proprioceptive information. Therefore, the visual weight in each of the visual and proprioceptive coordinates is calculated as:

$$\alpha_{MV} = \sum_{IHP,v}\sum_{V,v}^{-1} \quad (13)$$

$$\alpha_{INV} = \sum_{IHP,p}\sum_{V,p}^{-1}, \quad (14)$$

where α_{MV} is the multisensory integration weight for visual information in visual coordinates and α_{INV} is the multisensory weight for visual information in proprioceptive coordinates. Additionally, $\sum_{IHP,v}$ is the covariance matrix of IHP in visual coordinates, and $\sum_{V,v}$ is the covariance matrix of visual information in visual coordinates. Similarly, $\sum_{IHP,p}$ is the covariance matrix of IHP in proprioceptive coordinates, and $\sum_{V,p}$ is the covariance matrix of visual information in proprioceptive coordinates.

Final Motor Command and Movement Direction

After estimating the IHP, the desired movement vector is calculated by subtracting the hand position from the target positon: $\Delta x = \text{tar} - \mu_{IHP,v}$. We used the velocity command model (Burns and Blohm 2010; Sober and Sabes 2003) to transform the desired movement vector to the required motor command: $\dot{x} = J(\theta)J^{-1}(\hat{\theta})\Delta x$ {where J is the Jacobian of the system, θ is the actual joint configuration, and $\hat{\theta}$ is the estimated joint angle in the proprioceptive coordinates [$J(\theta)$ and $J^{-1}(\theta)$ have the same form as *Eqs. 16* and *17* in Burns and Blohm (2010)]}.

At the final step, the movement direction is calculated by transforming the movement command from Euclidean coordinates to polar coordinates using the following equations:

$$r = \sqrt{x^2 + y^2} \quad (15)$$

$$\tan\varphi = \frac{y}{x}. \quad (16)$$

Generating Quantitative Model Predictions

To generate our model predictions, we used a Monte Carlo approach (Binder and Heermann 2002); we assumed that the sensory information (visual and proprioceptive information of initial hand position and visual/vestibular and proprioceptive information of head position) can be sampled from a Gaussian distribution with a specific mean and covariance matrix. Then, the RFT procedure is performed on each sample based on sampled HR signals to obtain the distribution of the transformed signal. The movement direction was calculated for each sample, and the final movement mean and variance were calculated based on this distribution. The model code is available on GitHub (see ENDNOTE).

Model Parameters

Based on average body physiology, upper arm and lower arm (including fist) lengths were set constant to L1 = 30 cm and L2 = 45 cm, respectively. Shoulder location was assumed 30 cm backward from the target and 25 cm rightward of the target, the distance between eye and top of the head considered 13 cm, and the head length considered 28 cm (40 cm including the neck). IHPs and target positions were taken from the experimental data.

There were seven free parameters in the model, i.e., the variance of both proprioceptive (σ^2_p) joint angles and visual IHP (σ^2_v)–we assumed that the two dimensions in both coordinates are independent with the same variability: the visual/vestibular vs. neck muscle spindle contribution factor (C), the variance of head angle estimation for head straight (σ^2_{h0}), a fixed RFT cost (σ^2_{fT}), and a variable RFT cost (σ^2_{VT}).

As mentioned before, σ^2_{VT} resulted from the variability in the head angle estimation, δ^2_{HA}. By substituting $C = \delta^2_{NM}/\delta^2_{V/V}$ in *Eq. 7*, we were able to extract the variance of neck muscle spindles (σ^2_{NM}) and visual/vestibular ($\sigma^2_{V/V}$). Furthermore, we added an additional variance

component to account for the added variability during performing the planned movement (σ^2_{MV}).

To estimate the model parameters, we used a standard maximum likelihood procedure. We calculated the negative log-likelihood of the angular reach error data to fit on the proposed model given parameter set ρ as:

$$L_\rho(\mu, \sigma^2 | y) = -\left[-\frac{n}{2}\ln(2\pi) - \frac{n}{2}\ln(\sigma^2) - \frac{1}{2\sigma^2}\sum_i (y_i - \mu)^2 \right], \quad (17)$$

where (μ, σ^2) are the mean and variance driven from the model given the parameter set ρ, n is the number of data points, and y_i is each data point from the experiment. It should be noted that (μ, σ^2) are calculated separately for each of the 360 experimental conditions: 8 visual targets × 5 IHPs × 3 HRs × 3 NLs. We then searched for the set of parameters, which minimized the L_ρ over the parameter space using "fmincon.m" in MATLAB 2017. Table 1 provides the fitting values for different model parameters for individual participants along with the confidence interval for each parameter.

RESULTS

Previous studies (Burns and Blohm 2010; Schlicht and Schrater 2007; Sober and Sabes 2003) suggest that human behavior is affected by stochastic RFTs. Burns and Blohm (2010) showed that HR increases the variability of reach movements and argued that it could be due to the signal-dependent noise in the sensed head angles; HR increases the amplitude of the sensed head angle and the associated variability accordingly, which results in noisier RFTs. Here, our goal was to investigate the sources of stochasticity in RFTs and the effect of such stochasticity on human reaching movements. To this aim, we asked human participants to perform reaching movements while their head was either straight or rolled toward each shoulder and an NL of 0 or 1.8 kg was applied to the right or left side in a 3 × 3 design. The experimental logic was that applying HR and NL will vary the sensed head angle and the associated noise due to signal-dependent noise. Since RFTs are based on these sensed angles, applying HR/NL increases the stochasticity of RFTs, which modulates the multisensory integration weights and thus results in more variable and potentially biased reaching movements compared with the condition where the head is straight and no load is applied.

General Observations

A total of 51,840 trials were collected, with 1,529 trials being excluded due to either eye movements (participants were instructed to fixate their eyes on the center cross) or predictive hand trajectories. We used directional reach errors to determine how participants weighted their visual information vs. proprioceptive information. Directional reach error (in angular degrees) was computed by subtracting proprioceptive (visual) hand-target direction from overall movement direction (see MATERIALS AND METHODS), where 0° means no deviation from proprioceptive (visual) hand-target direction. By introducing the shift in the visual feedback of the initial hand position, a discrepancy between visual and proprioceptive information was created, and, as a result, we could determine how visual and proprioceptive information was weighted and integrated based on how participants responded to this discrepancy.

To evaluate how humans weight visual and proprioceptive information, we compared reach errors for each hand offset condition. Reach errors are calculated for each target by subtracting the actual (proprioceptive) hand-target direction (lighter gray line in Fig. 1*B*) or visual hand-target direction (darker gray line in Fig. 1*B*) from the performed reach movement. We called the first one proprioceptive reach errors and the second one visual reach errors and used them for different sections of this article to show the effects more clearly. The difference in reach errors among different hand offsets indicates that both visual and proprioceptive information were used during reach planning. Figure 4 displays both proprioceptive and visual reach error curves across target directions for different initial hand position conditions for head straight and no load condition.

To quantify these weights, we fitted a previously proposed model (Sober and Sabes 2003) to the normalized data. The data

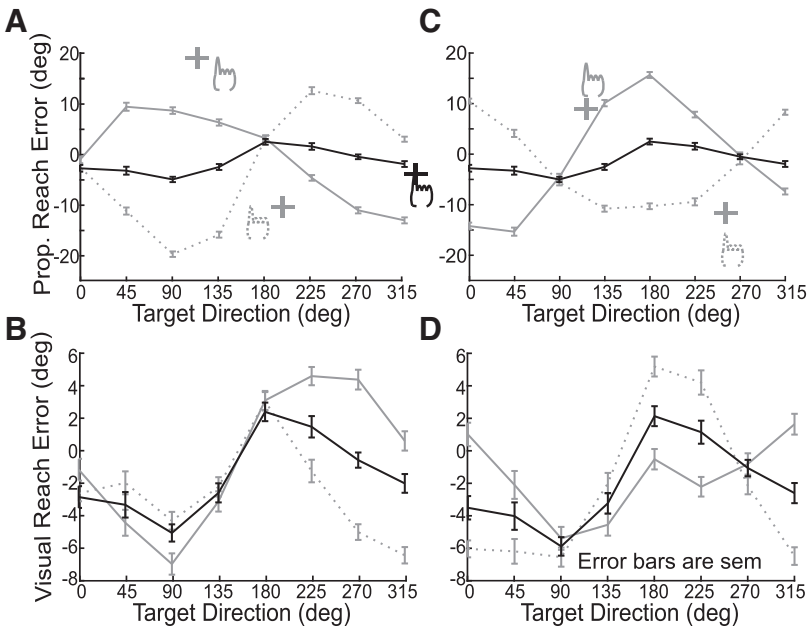

Fig. 4. Reach error curves. Reach errors are calculated for each target by subtracting the proprioceptive or visual hand-target direction from the performed reach movement. Solid lines represent upward/rightward shifts. *A* and *C*: proprioceptive (Prop.) reach error curves: reach errors for horizontal hand shift (*A*) and reach errors for vertical hand shift (*C*). *B* and *D*: visual reach error curves: reach errors for horizontal shift (*B*) and reach errors for vertical shift (*D*). deg, Degrees.

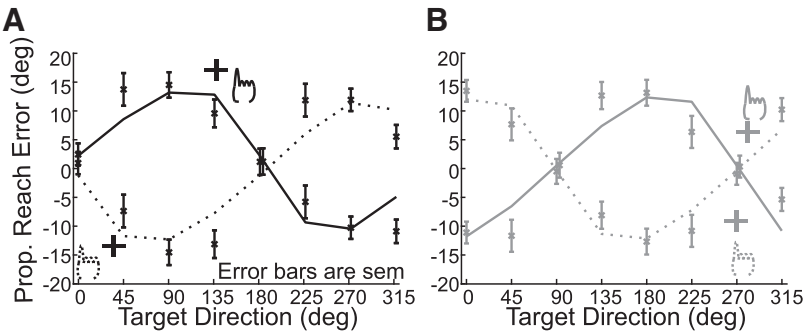

Fig. 5. Sober and Sabes (2003) model fit on the data. *A* and *B*: reach error curves are normalized to 0 by subtracting the 0 hand offset from the other hand offsets. deg, Degrees; Prop., proprioceptive.

were normalized by subtracting the 0 hand offset from the other hand offsets. The model by Sober and Sabes (2003) fits our data well (Fig. 5; r^2 for pooled data across all participants was equal to 0.91 and 0.93, respectively, for *A* and *B*) and confirms that the participants used both visual and proprioceptive information to plan their reach movements. Based on this close fit of our data to the model, we can now use this model in a first step to investigate how HR and NL affect the weighting of vision and proprioceptive information about the hand.

HR Effect

Participants performed the reach-out movements for different HR conditions: 30° counterclockwise (CCW), 0°, and 30° clockwise (CW) HR. In the first step, we examined whether the same effect reported by Burns and Blohm (2010) could be reproduced. As the authors explained, changing the HR had two different effects on the reach error trajectories. First, the reach error curves shifted up-/downward, and, second, the variability of reach errors increased for the tilted head conditions compared with the head upright condition.

Figure 6 depicts the effect of changing HR on both reach errors and movement variability. As can be seen, there are both a bias effect and an increased variability effect for altering the head orientation compared with head straight. The *n*-way ANOVA with factors HR, target directions, and participants showed a significant main effect for altering head orientation, $F(2,98) = 11.85$, $P < 0.01$, and significant interaction between reaching to different targets and different HR conditions, $F(14,98) = 5.59$, $P < 0.01$, which shows that the effect of altering HR is different for different target directions. Bonferroni-corrected post hoc analyses indicated that the bias effect was significant among all of the HR conditions. Regarding movement variability, we performed a paired *t*-test across all participants for each HR condition vs. no HR condition: the increase in standard deviation due to HR is significant for both sides, HR = 30° CW vs. HR = 0: $t(8) = -3.6133$, $P < 0.01$; HR = 30° CCW vs. HR = 0: $t(8) = -5.6011$, $P < 0.01$. These results are consistent with the results reported by Burns and Blohm (2010).

We also used the Sober and Sabes (2003) model to extract the weights for different conditions. There, the visual and proprioceptive weights were the two free parameters of the model (Sober and Sabes 2003), which are used to estimate the hand position, by integrating visual and proprioceptive information, in two different stages: visual weight at the movement planning stage (in visual coordinates) and visual weight at the motor command generating stage (in proprioceptive coordinates). Therefore, the weights can be extracted after fitting the model on the data. As is depicted in Fig. 6, the visual weights in visual coordinates did not change very much by varying HR; however, the visual weight in proprioceptive coordinates decreased for HR conditions. This is consistent with our hypothesis that higher noise in RFTs results in lower reliability of transformed signals, which leads to higher weights for proprioceptive information in the proprioceptive coordinates compared with the head straight condition.

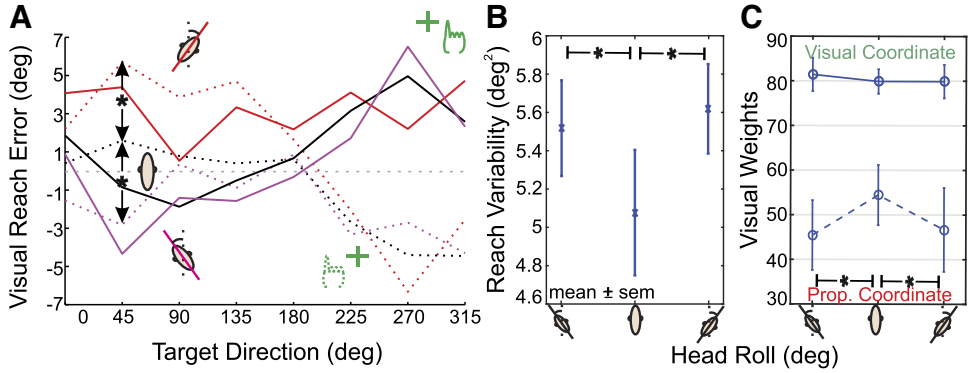

Fig. 6. Effect of varying head roll on reach movement behavior. *A*: reach error curves [solid line for initial hand position (IHP) shifts to right and dotted line for IHP shifts to left] shifted upward for clockwise head roll and downward for counterclockwise head roll compared with the head upright condition [*n*-way ANOVA, $F(2,98) = 11.85$, $^*P < 0.01$]. *B*: movement variability increased significantly for rolled head conditions compared with the head upright condition (paired *t*-test, $^*P < 0.01$). *C*: visual weights derived by fitting the Sober and Sabes (2003) model on the data. We did not find any significant change in visual weights in visual coordinates for different head roll conditions, whereas the visual weights significantly decreased in proprioceptive (Prop.) coordinates. Significance was tested using paired *t*-test ($^*P < 0.05$ is considered as a significant difference). deg, Degrees.

NL Effect

In addition to altering the HR, an NL (rightward, no load, or leftward) was applied. We assumed that if the NL was not taken into account, there should be no difference in the reach errors between the NL conditions and no load condition. Alternatively, if the NL was taken into account in estimating HR, we expected to observe similar effects as during HR: up-/downward shifts in reach error curves and increased movement variability. This is because applying an NL while the head is upright would create a discrepancy between the neck muscle spindle information and the combined visual/vestibular information. In addition, due to signal-dependent noise, the neck muscle information should become less reliable when the neck is loaded compared with the no load condition. Consequently, the sensed head angle estimated by integrating neck muscle and visual/vestibular signal should be biased toward the NL and have more variability, resulting in biased and more variable movements.

As can be seen in Fig. 7*A*, applying the NL created an up-/downward shift of the reach movement error curves. An *n*-way ANOVA with factors NL, target location, and participants revealed a significant main effect for different NL, $F(2,98) = 6.12$, $P < 0.01$. Bonferroni-corrected post hoc analyses indicated that the bias effect was significant among all of the NL conditions. The interaction between targets and different NL was not significant, $F(14,98) = 1.06$, $P = 0.402$, which means that the effect of varying NL on reach movement was independent of different target directions.

Figure 7*B* represents the variability of reach errors in the no load condition vs. NL conditions. As the figure demonstrates, the variability of reach errors is higher for applying the load compared with no load condition. We performed paired *t*-tests between all three different conditions across all eight participants. Movement variability was significantly higher for applying the load on the left side compared with no load condition, $t(8) = 2.7552$, $P = 0.0283$. The paired *t*-tests revealed no significant difference among other conditions.

Comparison

So far, we showed that there are both biases and increased movement variability effects for either applying NL or HR. In the next step, we compared the variability of reach movements in the NL conditions vs. HR conditions. Based on stochasticity in RFTs, we expected to have higher variability for higher amplitudes of head angle during different experimental conditions. For example, we predicted to have higher movement variability for applying only HR compared with applying only NL or have the highest variability for conditions in which both HR and NL are applied in the same direction.

Based on Fig. 8, the variability in HR conditions is higher than in NL conditions. We first ran paired *t*-tests between each condition separately, and the significant statistical differences are shown in the Fig. 8. Applying the load on the left side increased the variability compared with the control condition. Then, we performed paired *t*-test between combined similar conditions: for example, both head upright and NL on either side are combined and created the overall NL condition. The paired *t*-test between HR condition and NL condition showed a significant difference, $t(8) = 2.7444$, $P = 0.0287$; the difference between HR condition and control condition was significant as well, $t(8) = 2.7444$, $P = 0.0020$; however, the difference between the control and NL conditions was not significant. Together, all of the above observations provide evidence for the existence of signal-dependent noise in the head angle estimation and consequently the RFT processes. However, it is not clear how such stochastic RFTs affect the reaching movement. First, contrary to the initial hypothesis, no modulation of variability was observed by varying NL while the head was rolled CW/CCW. In addition, in all of the conditions, we observed larger effects when HR on reach errors for targets away from the body (45–135°) compared with the targets toward the body (215–315°). Both previous models (Burns and Blohm 2010; Sober and Sabes 2003) fail to explain the mentioned effects; both previous models predict constant up-/downward shift due to HR for all target positions. We propose that these effects can be explained by a Bayesian framework, which performs geometrically accurate RFTs.

Modeling the Stochastic RFTs

The above analyses demonstrate that RFTs should be considered as stochastic process. Therefore, to understand the effect of such stochastic RFTs on reach planning, we devel-

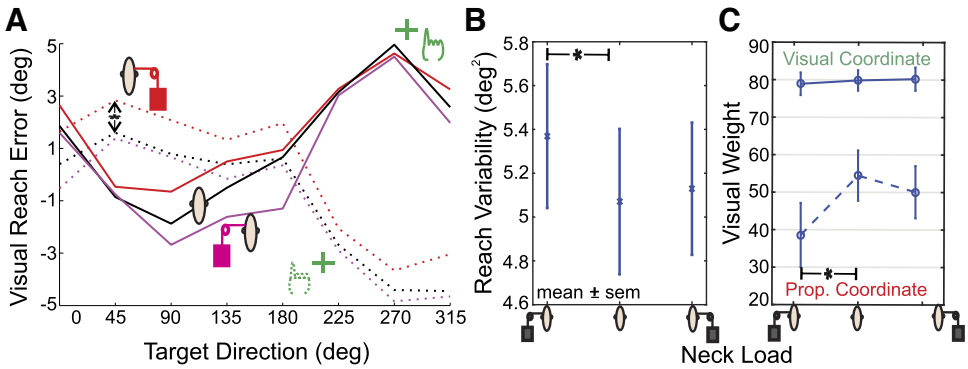

Fig. 7. Effect of applying neck load on reach movement behavior. *A*: reach error curves [solid line for initial hand position (IHP) shifts to right and dotted line for IHP shifts to left] are shifted upward for applying neck load on the right [*n*-way ANOVA, $F(2,98) = 6.12$, $^*P < 0.01$]. Shift in reach error curves for applying neck load on left is not statistically significant. *B*: movement variability is increased significantly for applying the load on the left compared with the no load condition [paired *t*-test, $t(8) = 2.7552$, $^*P = 0.0283$]. *C*: visual weights derived by fitting the Sober and Sabes (2003) model on the data. We only observed a significant change in visual weight in proprioceptive (Prop.) coordinates due to applying neck load on the left side. Significance was tested using paired *t*-test ($^*P < 0.05$ is considered as a significant difference). deg, Degrees.

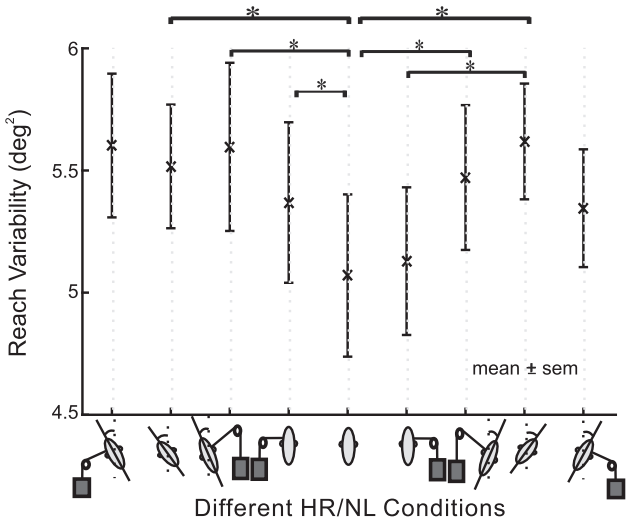

Fig. 8. Effect of different experimental conditions on reaching movement variability. Head upright and no load condition (considered as the control condition) and the combined head roll and neck load (HR/NL) conditions are sorted based on the expected increase in the variability based on the signal-dependent noise hypothesis right and left of the control condition. Rolling the head consistently increased the variability compared with the control condition. Significance was tested using paired *t*-test (*$P < 0.05$ is considered as a significant difference). deg, Degrees.

oped a Bayesian model of multisensory integration for reach planning and explicitly included the RFTs.

Figure 3 depicts the schematic of our proposed model. The working principles of our model are similar to previous ones (Burns and Blohm 2010; Sober and Sabes 2003) with the addition of an explicit head orientation estimator (Fig. 9, blue box). In summary, our model calculates the required reach movement through first calculating the movement vector in visual coordinates, by comparing estimated initial hand position and target position, and then generates the movement commands by transforming the movement vector from visual coordinates to proprioceptive coordinates.

We added several crucial features to the proposed model compared with the previous models (Burns and Blohm 2010; Sober and Sabes 2003). First, we explicitly included the RFTs. The RFT processes transforms information between different coordinates considering the full-body geometry: head orientation, eye orientation, head-eye translation, and head-shoulder translation. In addition, to perform the required transformations, we included a head angle estimator. The head angle estimator combines muscle spindle information and visual/vestibular information in a statistically optimal manner. Similar to Burns and Blohm (2010), we modeled both mean behavior and the associated variability for each source of information: vision, proprioceptive, vestibular, and muscle spindles. To examine the effect of noisy transformations on the visual/proprioceptive information, we deployed Monte Carlo simulations. This method gave us the opportunity to study explicitly the effect of RFTs on the covariance matrices and consequently the multisensory integration weights.

Model Fit

In the following section, we first provide the fitting results for a sample participant (*S6*) and then evaluate the fitting results across all nine participants. Figure 9 provides the fitting vs. data for *participant S6*. Figure 9, *A* and *B*, depicts model fitting for all different initial hand positions for different HRs while no NL was applied. As can be seen, our model is able to capture the reach errors for different IHP and HR conditions accurately. Figure 9*C* provides the model prediction for changes in variance for different conditions. Error bars were derived using bootstrapping with $n = 1{,}000$. Since the results for horizontal and vertical hand shifts are very similar, for all of the other conditions, we only provided the results for the horizontal initial hand shifts (Fig. 9, *D–F*). Figure 9, *D–F*,

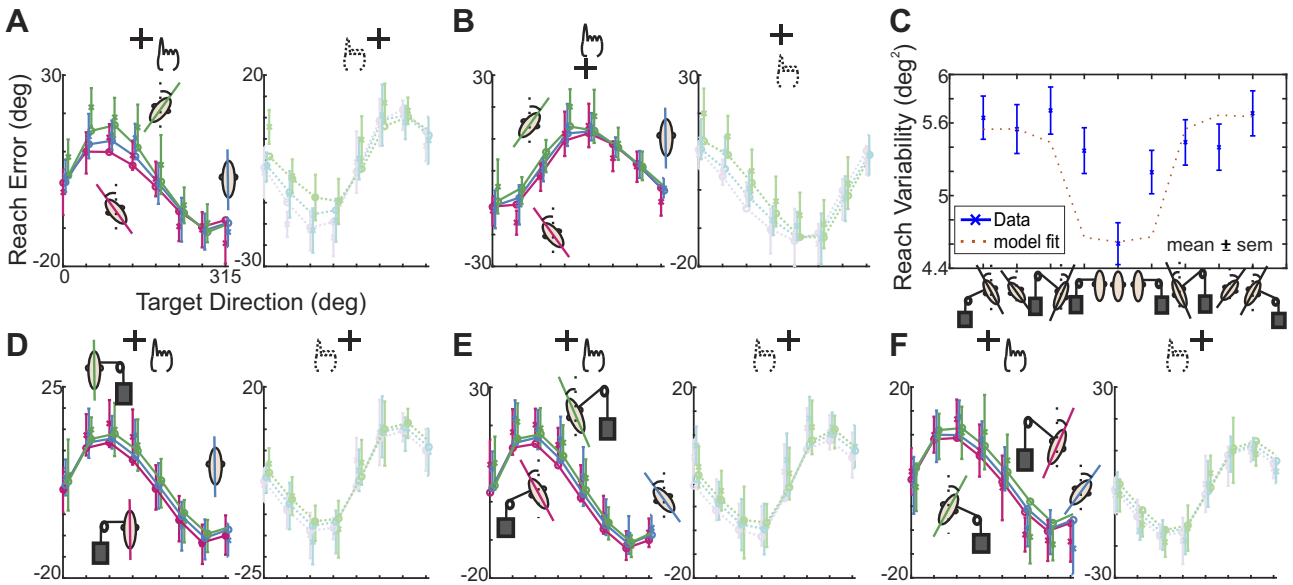

Fig. 9. Model fit for a sample participant (*S6*). Model fits on the reach error curves for different initial hand positions (IHPs) and head roll (HR) and neck load (NL) conditions is shown. *A* and *B*: model fit on the reach error curves for varying head orientation without applying neck load: solid line represents results for IHP shifts to the right, and dotted line represents results for IHP shifts to the left (*A*); solid line represents results for IHP shifts up, and dotted line represents results for IHP shifts down (*B*). *C*: model fit on the changes in movement variability due to varying HR and NL conditions. *D–F*: model fit on reach errors for varying NL for different HR conditions. Only data for horizontal shifts are presented. Results for vertical hand shifts are similar. deg, Degrees.

Table 1. *Model parameter fits*

Participant	σ_p^2, rad^2	σ_v^2, mm^2	σ_{fT}^2, mm^2	$\sigma_{V/V}^2$, deg^2	σ_{NM}^2, deg^2	σ_{h0}^2, deg^2	C	σ_{MV}^2, mm^2
S1	4.69×10^{-4}	13.50	56.68	3.04×10^{-2}	7.89×10^{-1}	5.66	25.92	100.87
S2	4.86×10^{-4}	21.59	56.10	1.49×10^{-1}	3.87	5.61	25.76	48.53
S3	4.86×10^{-4}	16.50	56.72	1.54×10^{-1}	4.00	5.79	26.00	49.00
S4	3.11×10^{-4}	9.01	32.71	2.36×10^{-1}	5.92	4.97	25.13	11.56
S5	2.45×10^{-4}	15.00	26.86	1.08×10^{-1}	2.81	5.00	25.98	95.75
S6	4.81×10^{-4}	15.03	38.78	1.23×10^{-1}	3.20	5.77	26.00	37.97
S7	4.84×10^{-4}	20.97	38.81	3.07×10^{-1}	7.97	5.80	25.91	26.99
S8	2.87×10^{-4}	16.09	38.44	1.18×10^{-1}	3.08	5.80	26.00	41.32
S9	3.20×10^{-4}	18.99	38.58	2.97×10^{-1}	7.68	5.74	25.89	26.98
95% CI	$[3.13, 4.80] \times 10^{-4}$	[13.12, 19.47]	[33.57, 51.69]	$[0.94, 2.44] \times 10^{-1}$	[2.44, 6.30]	[5.30, 5.85]	[25.61, 26.07]	[23.93, 73.62]

σ_{fT}^2, fixed-transformation variance; σ_{h0}^2, baseline head angle estimation variance; σ_{MV}^2, movement variance; σ_{NM}^2, neck muscle spindle variance; σ_p^2, proprioceptive variance; σ_v^2, visual variance; $\sigma_{V/V}^2$, visual/vestibular variance; C, contribution factor; CI, confidence interval; deg, degrees; *S*, subject number.

depicts the fitting for varying the NL for different head angles: 0°, ± 30°.

After demonstrating that our model was capable of predicting the reach error behavior for a single participant, Table 1 summarizes the fitting results for all of the participants. The most interesting finding here is the relatively higher contribution of visual/vestibular signal compared with neck muscle spindle (C ≈ 26). This was consistent across all of the subjects. We also observed very high movement variability across our participants.

Figure 10 provides the model prediction vs. data for both reach errors and variances for different experimental conditions. Different participants are differentiated by different colors. We used several different analyses to evaluate the goodness of our model fit. First, we calculated r^2 value for each individual participant and the pool of all of the participants: (54, 61, 56, 75, 50, 60, 66, 71, 71, and 94) for *S1–S9* and the pool of data, respectively. Second, since the variance data were very noisy, we grouped them in bins and calculated the confidence interval for each predicted variance using the following equation (Williams 1962):

$$\frac{(n-1)\times s^2}{\chi^2_{\alpha/2}} \le \sigma^2 \le \frac{(n-1)\times s^2}{\chi^2_{1-\alpha/2}}, \qquad (18)$$

in which σ^2 is the population variance, s^2 is the sample variance, n is the sample size, and $\chi^2_{\alpha/2}$ is χ^2-distribution. Since we wanted to find the 95% confidence interval, we set $\alpha = 0.05$. The boxed colored area in Fig. 10, *B* and *C*, is the calculated confidence interval for the variances. Based on this analysis, we could see that our model provides a decent fit on the data.

Finally, we examined whether our residual has a random pattern by examining the normality of our model residual using normal probability plot, plotted using MATLAB 2016 "normplot.m." Figure 11 provides the normal probability plot of our fitting for all nine participants. As depicted, residual values for all of the participants approximately have a normal distribution, which implicates that our model captures all of the features in the data. More details of how our model explains the data can be found in APPENDIX.

DISCUSSION

We assessed the effect of neck muscle spindle noise on multisensory integration during a reaching task and found that applying NL biased head angle estimation across all HR angles, resulting in systematic shifts in reach errors. We also examined the effect of HR on reach errors and observed both an increase in movement variability and biases in reaching errors, similar to Burns and Blohm (2010). To examine the effect of noise on reaching movements quantitatively, we developed a novel 3D stochastic model of multisensory integration across reference frames. The effect of neck muscle spindle noise and HR could be

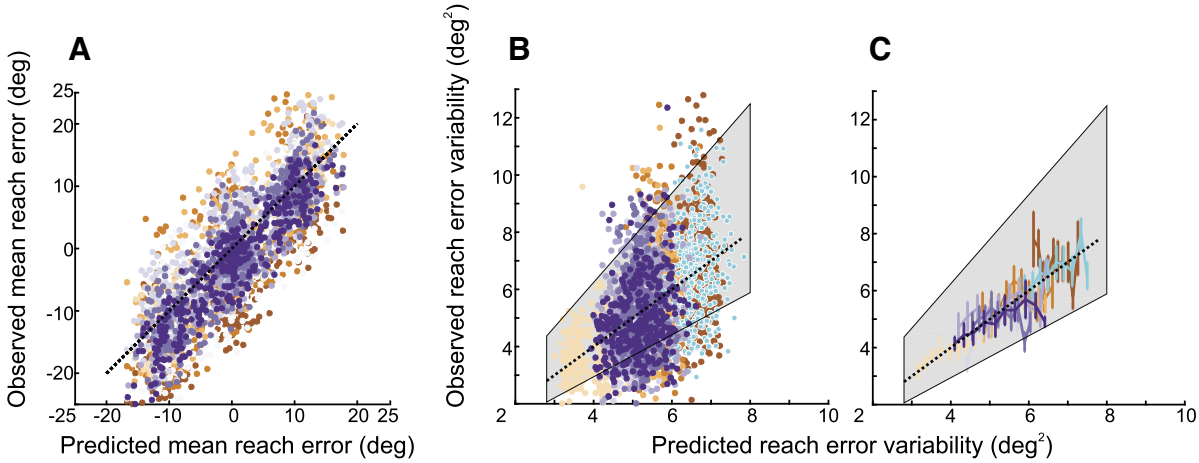

Fig. 10. Model prediction vs. observed data for each individual participant. Data for each individual participant was fitted to our model. Each color represents an individual participant. *A*: model prediction vs. observed data for reach errors. *B*: model prediction vs. observed data for reach variability. *C*: same data as in *B* grouped into bins of 0.25 deg^2 (mean and standard error). Gray box represents the confidence interval for predicted variances based on our model. deg, Degrees.

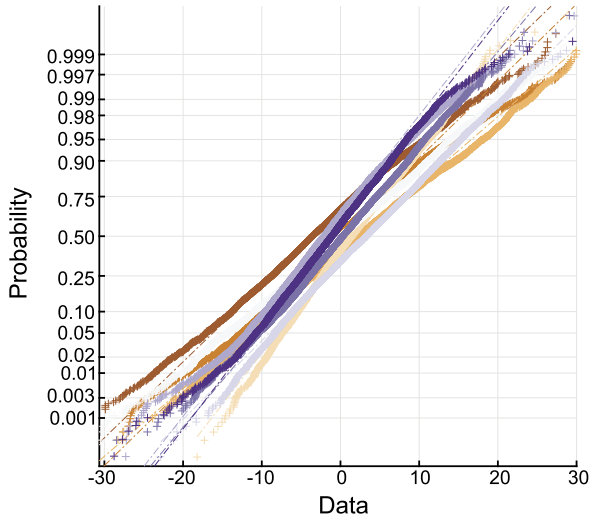

Fig. 11. Residual analysis: normal probability plot. Probability plot is depicted for each participant different colors. As can be seen, the residual of our model fit compared with the participants' data has almost a normal distribution for all of the participants.

explained by a misestimation of head orientation and signal-dependent noise in the RFTs between visual and proprioceptive coordinates. The model was able to reproduce successfully the reaching patterns observed in the data, providing evidence that the brain has online knowledge of full-body geometry as well as the reliability associated with each signal and uses this information to plan the reach movement in a statistically optimal manner.

Model Discussion

In our model, the multisensory integration process occurs in specific reference frames, i.e., in visual and proprioceptive coordinates. Therefore, signals should be transformed into the appropriate coordinate frame before integration, which is done by a series of coordinate rotations and translations. However, we do not claim that the brain performs these computations in the same explicit serial way. Alternatively, neurons could directly combine different signals across reference frames (Abedi Khoozani et al. 2016; Beck et al. 2011; Blohm et al. 2009; Ma et al. 2006), e.g., by gain modulation mechanisms. Regardless of the mechanism used, we expect very similar behavioral outcomes.

In addition, we assumed that all of the distributions remain Gaussian after performing RFT processes to simplify the required Bayesian computations. However, in general, this is not necessarily correct. For example, it has been shown that noisy transformations can dramatically change the distribution of transformed signals (Alikhanian et al. 2015). Since the noise in our RFTs was small enough, the deviations from a Gaussian distribution are negligible, and this approximation did not affect our model behavior dramatically. It would be interesting, however, to examine how considering the actual distribution and performing the basic Bayesian statistics (Press 1990) will change the model behavior.

Finally, properly fitting 7 free parameters requires cautious considerations of 2 main challenges. The 1st is the problem of overfitting, which we believe was not a problem in our study. Overall, we had 288 conditions, including 4 variations of initial hand position, 8 visual target positions, and 9 HR and NL combinations. Therefore, we had enough conditions and data points to fit our 7-parameter model accurately. The 2nd challenge is how to interpret the values of the fitted parameters. We believe the consistency of fitted values across participants illustrates the reliability of the approach. For our purpose and to get insight into the mechanisms underlying our experimental findings, we were mostly interested in the relative importance of visual and proprioceptive signals and how those were affected by HR. Thus we believe that our 7-parameter model provides a concise mechanistic explanation of the data.

Interpretation of Observations

We suggest that NL biased head angle estimation across all HR angles, which resulted in systematic biases in reach error curves. Our model accounted for these shifts by assuming that NL biases the head angle estimation toward the direction of the load. It has been demonstrated that the brain can estimate head orientation by combining vestibular, visual, proprioceptive, and efference copy signals. The vestibular system and especially otolith system is very important for estimating the static head orientation relative to gravitational axes (Fernandez et al. 1972; Sadeghi et al. 2007). Vingerhoets et al. (2009) demonstrated that tilted visual and vestibular cues bias the perception of visual verticality. The authors showed that a Bayesian model that integrates visual and vestibular cues can capture the observed biases in verticality perception. Furthermore, muscle spindles play an important role in determining joint position sense (Goodwin et al. 1972; Scott and Loeb 1994) compared with the other sources, e.g., tendons or cutaneous receptors (Gandevia et al. 1992; Jones 1994). Armstrong et al. (2008) showed that the muscles in the cervical section of the spine have a high density of muscle spindles providing an accurate representation of head position relative to the body. Finally, previous studies have provided evidence that the contribution of efference copy is only relevant during movement and decreases toward the end of a movement (Medina et al. 2010). Therefore, head angle can be estimated from a combination of visual, vestibular, and neck muscle spindle information.

We included multisensory integration of visual/vestibular and neck muscle spindle signals in our model. Since we only modulated neck muscle information, we assumed that a combination of visual/vestibular signals is integrated with neck muscle spindle information. We were able to retrieve the relative contribution of visual/vestibular information vs. neck muscle spindle information by fitting our model to the data. We found that the contribution of neck muscle spindle information was very low (in the order of 5%) compared with visual/vestibular information.

There could be several possible explanations for observing a relatively low contribution of the neck muscle information. First, we selected the amount of the NL in a way to apply force comparable with 30° head tilt. However, due to the complex organization of neck muscles (Armstrong et al. 2008), we could not directly measure the changes in muscle activity. Therefore, to measure the effect of applying load on neck muscle spindle information accurately, a detailed model of neck muscle organization would be required. From our design, it was not possible to dissociate muscle spindle information from other proprioceptive information. Consequently, the results provided here can be considered as the overall proprio-

ceptive information (neck muscle spindle, skin receptors, et cetera). Moreover, usually neck muscle information agrees with the skin receptor (i.e., cutaneous receptor) information. In our task, however, the neck muscle information and cutaneous receptor information are in conflict, which might be a potential reason for downweighting neck proprioceptive information (Körding et al. 2007).

Unexpectedly, we observed that applying HR creates larger reaching movement biases for visual targets away from the body compared with visual targets toward the body. This pattern can be captured by including the full-body geometry in the RFT processes in our model. Previously, Blohm and Crawford (2007) showed that to plan a reaching movement to visual targets accurately, the full-body geometry (both rotations and translations) has to be taken into account by the brain. Based on our model, the displacement of centers of rotation between head- and eye-centered coordinate spaces caused this asymmetry in the reaching movements.

In addition to biases, we observed that reaching movements were more variable in the straight head with NL conditions compared with the straight head and no load condition. We considered this as evidence for NL affecting RFTs; we assumed that the neck muscle spindles have signal-dependent noise (Scott and Loeb 1994). Therefore, applying the NL increases the noise in the neck muscle spindle information and consequently the sensed head orientation. This noisier sensed head angle resulted in noisier RFTs and accordingly more variable reach movements.

Surprisingly, we observed an asymmetry in the amount of variability increase by applying NL on the right vs. left side when the head was upright. One explanation could be that since all participants were right-handed, they were more sensitive to the changes on the left side. Several imaging studies demonstrated that right-handed people have bigger left hemispheres with more neural resources associated with the right side of the body (Bauermeister 1978; Linkenauger et al. 2009a, 2009b). Bauermeister (1978) tested the effect of handedness on perceiving verticality and showed that right-handed participants are more responsive to the right-sided stimulus than to the left-sided stimulus.

Since HR with no NL caused higher increase in movement variability compared with applying NL while the head was upright, we expected to see a systematic modulation of movement variability by applying NL while the head was tilted. Specifically, we expected to observe the highest amount of movement variability when the NL and HR were applied on the same side, e.g., 30° CW HR and right-side NL. The logic is that when both HR and NL are applied in the same direction, the neck muscle signal indicates the highest angle, and due to signal-dependent noise the associated variability of head angle estimations has the highest value. However, applying the load on the same side as the tilted head did not increase the movement variability significantly compared with only tilting the head.

A possible explanation for the lower effect of applying load on the same side of titled head can be relatively low contribution of neck muscle spindle information vs. visual/vestibular information during head angle estimation, provided by our model. The remarkable observation is that even though the contribution of neck muscle information is low, applying NL still has a tangible effect on reaching movements for all HR conditions, observed both in our data and model predictions. Another explanation is that the brain might not integrate the visual/vestibular information in this condition due to the big discrepancy between neck muscle information and visual/vestibular information (due to lack of causality; Körding et al. 2007). In our experimental design, we selected the NL value to simulate the same force as when the head is titled 30° [head weight $\times$ sin(60°) = 0.5 $\times$ head weight]. Consequently, when the head is tilted 30° CW and the load is applied on the right side, the total force on the neck muscle can be calculated as 0.5 $\times$ head weight (head tilt) + 0.5 $\times$ head weight (head load) = full head weight; this force is stimulating the neck muscle as if the head were tilted 90°, which is very unlikely. Therefore, the brain might ignore the neck muscle spindle information fully.

We interpreted the observed increase in movement variability as an indication of signal-dependent noise in the RFT process. However, an alternative hypothesis to the signal-dependent noise is uncommon posture (Sober and Körding 2012). According to the uncommon posture hypothesis, we might have more neuronal resources allocated to the head straight posture since we perform most of our movements with the head straight. As a result, HR creates higher uncertainty due to uncommon posture independent of signal-dependent noise. Even though this argument might be valid for HR, it cannot explain the increased movement variability due to applying NL. In other words, applying NL while the body posture was kept unchanged still increased the movement variability, which is in contrary to the uncommon posture hypothesis.

We observed that changing HR and/or applying NL modulated multisensory weights in both visual and proprioceptive coordinates. We validated this finding by both fitting Sober and Sabes' (2003) model and our new full Bayesian RFTs model to the data. We found that increasing the noise in the sensed head angle estimation decreased the reliability of transformed signals, which we hypothesized is the result of the stochastic RFTs, and consequently lowered weights for transformed signals in the multisensory integration process. Therefore, we conclude that both body geometry and signal-dependent noise influence multisensory integration weights through stochastic RFTs.

We demonstrated that head position estimation plays a vital role in RFT processes required for reach movements. Previous studies showed that nonvisual information of head position in space, i.e., from the neck muscle spindles (Proske and Gandevia 2012) and from the vestibular system (Angelaki and Cullen 2008; Cullen 2012), declines over time, providing better information about the relative changes in head position than about the absolute position. This behavior is explained based on proprioceptive drift; afferent discharges decline over time (Tsay et al. 2014), resulting in imprecise absolute estimation of the head position. We evaluated the temporal evolution of head angle estimation and its possible effect on reaching movements by dividing each block of our experiment into four bins (data not shown); however, we found no changes in movement biases or variability. Therefore, we believe that our experimental design and timing were not appropriate to investigate changes of head angle estimation over time on reaching

behavior. This question, however, is an intriguing one and should be investigated in future experiments.

Implications

Our findings have implications for behavioral, perceptual, electrophysiology, and modeling studies. First, we have demonstrated that both body geometry and stochasticity in RFTs modulate multisensory integration weights. It is possible that other contextual variables such as attention or prior knowledge also modulate multisensory weights and will subsequently affect both perception and action. In addition, we have shown that such modulations in multisensory weights can create asymmetrical biases in reach movements. Such unexpected biases may be prevalent in behavioral data obtained during visuomotor experiments in which participants perform the task in a robotic setup while their body is in various geometries, e.g., tilted head forward or elevated elbow. Therefore, it is important to consider that forcing specific body configurations can create unpredicted effects that are important for interpreting the behavioral data.

Our findings also suggest that the brain must have online knowledge of the statistical properties of the signals involved in multisensory integration. This could be achieved by population codes in the brain (Ma et al. 2006), which agrees with the current dominant view that the brain performs the required computations through probabilistic inferences (Pitkow and Angelaki 2017). Alternatively, multisensory weights and the change of weights with contextual parameters could be learned (Mikula et al. 2018). Learned weights could be especially advantageous when it is difficult to estimate sensory reliability. Computational models that include required latent variables are crucial to understand the required computations. An important benefit of such models is that they can be used to generate training sets for neural networks to investigate potential neural mechanisms underlying probabilistic inference. Such studies will motivate appropriate electrophysiology experiments to validate/refute predictions of related models.

APPENDIX

Here, we provide more details of how our model performs RFTs on different sensory signals (modeled as Gaussian distributions). In our study, we demonstrated that the proposed model was able to replicate our behavioral data pattern (Fig. 9). In this section, we use the model to provide a mechanistic explanation of the observed reach movement patterns.

Sober and Sabes (2003) demonstrated that reaching errors caused by dissociating visual and proprioceptive information can be explained by two components: MV error that is the error at the vector planning stage and INV error, which is the error at the motor command generation stage. They showed that adding these two reaching errors leads to the error pattern observed in human participants. Furthermore, Burns and Blohm (2010) demonstrated that the observed up-/downward shifts in reaching error curves can be explained by RFTs; any misestimation in the sensed head angle results in an erroneous rotation of movement vector, which results in up-/downward shifts in reach error curves. The logic is the same in our model for explaining the observed biases in reach error curves for the HR condition. Similarly, the up-/downward shifts in reach error curves for the NL condition can be explained by erroneous RFTs; applying an NL biases the head angle, which leads to an erroneous rotation of the movement vector, resulting in shifts of error curves.

Applying an NL enabled us to evaluate the contribution of neck muscle spindle information to head angle estimation. To achieve this, we included a Bayesian head angle estimator in our model in which the visual/vestibular and neck muscle spindle information are integrated to estimate the head angle. Applying an NL biases the neck muscle spindle information toward the direction of the load and consequently biases the head angle estimation (*Eqs. 7* and *8*). This bias in estimated head angle depends on two parameters: *1*) relative neck muscle reliability compared with visual/vestibular reliability and *2*) overall head angle estimation variability [similar to the variable RFTs variance in Burns and Blohm's (2010) model].

As explained before, in our model, we estimate the head angle by integrating visual/vestibular information with neck muscle information. As a result, the overall sensed head angle variability depends on the variability of each of aforementioned information. Consider the situation in which overall head angle estimation variability is low (Fig. A1, *A* and *B*). Low variability for head angle estimation resulted from high reliability for both visual/vestibular and neck muscle spindle information. Similarly, high variability of head angle estima-

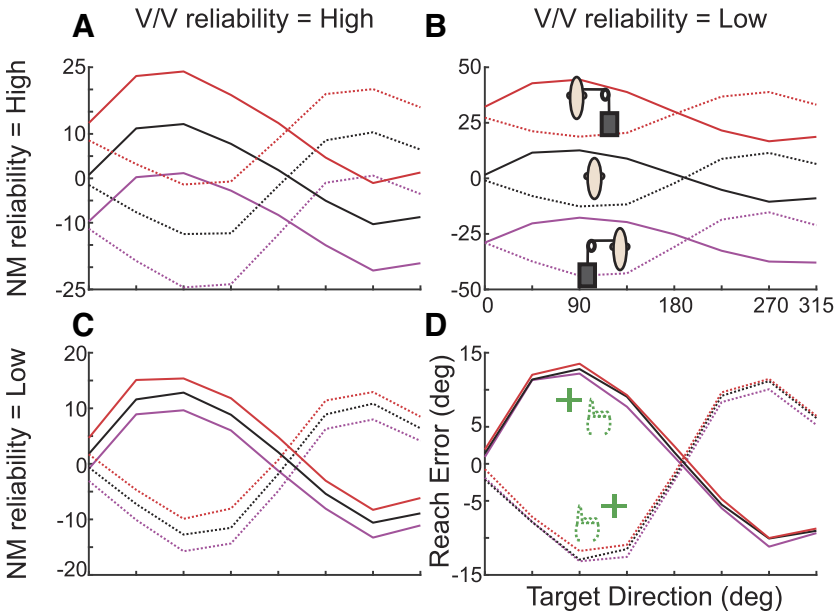

Fig. A1. Effect of varying the reliability of neck muscle (NM) spindle signals vs. visual/vestibular (V/V) signals. Head angle is estimated by combining the neck muscle spindle information with combined visual and vestibular information using the Bayesian method; therefore, the effect of applying neck load depends on 2 factors: *1*) absolute variability of head angle estimation and *2*) relative reliability of neck muscle spindle information compared with visual/vestibular information. *A* and *B*: lower absolute value for head angle estimation variability: this lower variability results from the high reliability of both visual/vestibular and neck muscle information. Therefore, the up-/downward shifts induced due to applying neck load are higher compared with when the head angle estimation variability is high (*C* and *D*). In addition to the absolute head angle estimation variability, the relative reliability of neck muscle spindle vs. visual/vestibular information impacts how much applying neck load biases the reaching movement. *A* and *C*: the lower the reliability of neck muscle spindle information vs. visual/vestibular information, the lower the up-/downward shifts in reaching error curves. *B* and *D*: increasing the relative reliability of neck muscle information increases the up-/downward shifts in reaching errors by applying neck load. deg, Degrees.

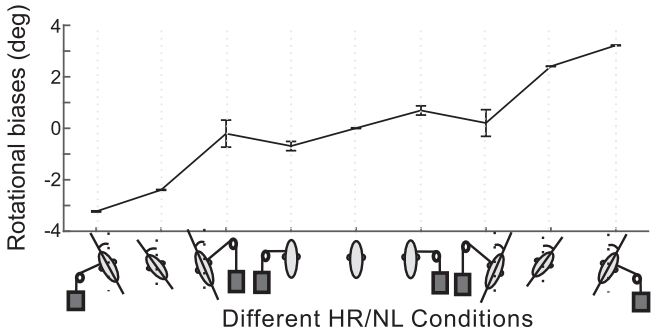

Fig. A2. Biases in head angle estimation due to different head roll (HR) and neck load (NL) conditions. Applying neck load biased the head angle estimation toward the applied load for all head angles. Error bars are standard deviations. deg, Degrees.

tion resulted from low reliability of both visual/vestibular and neck muscle spindle information, and consequently applying NL creates smaller biases (Fig. A1, *C* and *D*). We expect that applying an NL will create higher shifts in reach error curves for when the reliability of sensed head angle is high compared with when the reliability of sensed head angle is low, regardless of their relative contribution (compare Fig. A1, *A* vs. *D* and *B* vs. *C*).

In addition, the amount of shifts in reach error curves depends on the relative reliability of neck muscle spindle information vs. visual/vestibular information. When the relative reliability of neck muscle information is high, the bias in reach error curves is higher compared with when its reliability is low (Fig. A1, *B* vs. *C*). In our data, we observed high variability for head angle estimation as well as relatively higher contribution of visual/vestibular information compared with neck muscle spindle information ($C \approx 26$; Fig. A1*C*).

As mentioned before, at the heart of our RFT process, there is a head angle estimator, which enabled us to retrieve the sensed head angle based on the reach error patterns. Figure A2 demonstrates the biases in head angle estimation for all of the experimental conditions. As can be seen, applying NL biased the head angle estimation toward the applied NL for all head angles. We performed *t*-test analysis and observed that all of the changes in head angle estimation due to applying NL are significant: $-11 < t(8) < 12$, $P < 0.001$.

In addition to up-/downward shifts in reach error curves by applying NL and HR, we observed a very surprising pattern in our data: both HR and NL created greater biases in reaching movements when reaching to targets away from the body (45–135°) compared with reaching to targets toward the body (215–315°). This observation was surprising, and, to our knowledge, none of the previous models (Burns and Blohm 2010; Sober and Sabes 2003) could predict/explain this pattern.

At this point, it should come as no surprise that our model explains the difference in HR/NL effect for different targets by stochastic RFT processes. Blohm and Crawford (2007) demonstrated that the brain considers the full 3D body geometry to plan reach movements accurately. As mentioned in the model description, we included the 3D body geometry in our RFT procedure: RFT processes are carried out by sequential rotations/translations between different coordinates centered on different body sections.

Figure A3*A* demonstrates different coordinates that have been considered in our model in relation to each other. Including the 3D body geometry resulted in a displacement in the center of rotation between different coordinates and specifically in our experiment between gaze-centered and head-centered coordinates. This displacement of the center of rotation caused greater biases in reaching movements for visual targets further away from vs. closer to the body (Fig. A3*A*). Figure A3*B* provides a detailed example of how the difference in the center of rotation results in an asymmetry in the movement biases induced by HR/NL. The first block in Fig. A3*B* shows the actual scene in front of the participants with two targets at 90 and 270°.

In our experiment, the participants fixated their eyes on the cross, and this cross was indicated as their visual information of the initial hand position as well. In this example, the hand was shifted 25 cm horizontally to the right. The dotted arrows show the visual movement vector toward the targets. *Box 1* demonstrates the retinal representation of targets for 30° CCW HR. We assumed that the torsion effect on retinal information was small and, therefore, ignored it. Since the head is rotated 30° CCW, the retinal image on the back of the head is

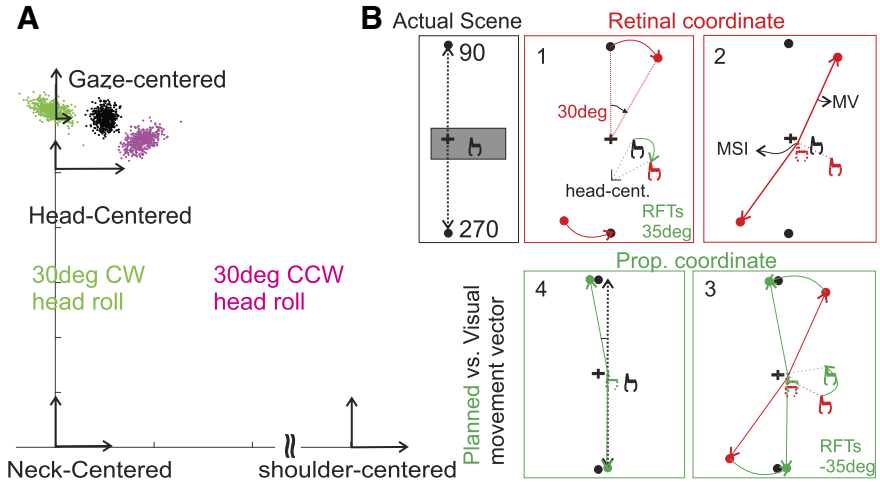

Fig. A3. Reference frame transformation (RFT) process mechanism. *A*: different coordinates in our RFT module. Difference in the center of rotation between gaze-centered coordinate and head-centered coordinate resulted in an asymmetry of transformed hand position for 30° clockwise (30deg CW) vs. counterclockwise (CCW) head rolls. *B*: detailed example of the higher effect of stochastic RFTs on movement away from the body compared with movements toward the body for 30° CCW head roll. Actual Scene: in our experiment, participants fixated their eyes on the center cross, and the visual feedback of the hand indicated their hand on the center as well. Actual hand position is shifted to the right in this example, and it is occluded. *Box 1*: retinal image of the target is rotated 30° CW; we ignored the torsion effects on retinal projection. Proprioceptive hand position is transformed using our RFT module (we assumed that head roll estimation is erroneous; 35°). head cent., Head-centered. *Box 2*: initial hand position is estimated by combining visual information and transformed proprioceptive information of the hand. Then, the movement vector (MV) is calculated by subtracting target position from the initial hand position. MSI, multisensory integration. *Box 3*: calculated movement vector is transformed to the proprioceptive (Prop.) coordinate using the RFT module. *Box 4*: comparing the planned movement with the movement only considering visual information. As can be seen, the misestimation in head angle created larger error for movement away from body vs. movement toward the body. This happened due to the offset in the center of rotations between different coordinates.

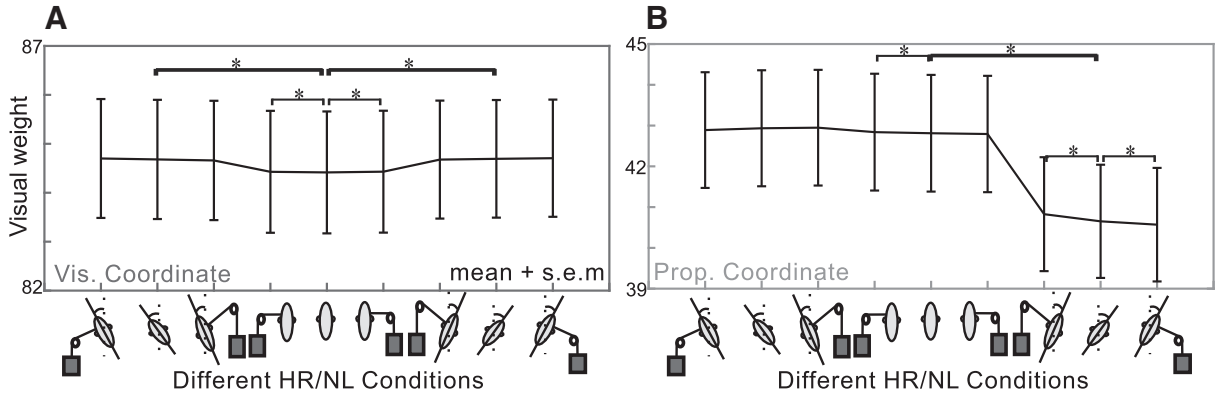

Fig. A4. Visual weights for multisensory integration. *A*: visual weights increase in visual (Vis.) coordinate due to decreased reliability of proprioceptive information caused by stochastic reference frame transformations. *B*: visual weights in proprioceptive (Prop.) coordinate: rolling the head 30° counterclockwise did not affect the visual weights, whereas rolling the head 30° clockwise decreased visual weights. The reason for this asymmetry is the nonlinearity in the inverse kinematic process. Error bars are standard error of the mean. *Significance was tested using paired *t*-test ($P < 0.05$ is considered as a significant difference). HR, head roll; NL, neck load.

rotated 30° CW (actual head angle), and the center of this rotation is the cross (gaze position). To estimate the hand position, proprioceptive information must be transformed to the retinal coordinates, and at the heart of this transformation is the head rotation based on the estimated head angle (blue box in Fig. 3). In this specific example, we assumed that the head angle is overestimated by 5° and is estimated as 35°. In addition, since the centers of rotation for head-centered and gaze-centered coordinates are different, the transformed hand position is no longer in symmetry with the rotation in gaze-centered coordinates and displaced and biased toward the body.

The next two steps in our model are multisensory integration to estimate the hand position and movement vector calculations (*box 2*). As has been shown by Sober and Sabes (2003, 2005), any transformation adds noise, and, therefore, visual information is more reliable in the retinal coordinates, the estimated initial hand position is biased toward the visual initial hand position, and the movement vector is calculated by subtracting target position from this estimated initial hand position. This movement vector, then, is transformed into shoulder-center coordinates to be executed, employing RFTs (*box 3*). We compared the transformed movement vector with the visual movement vector in *box 4*, and, as can be seen, the misestimation in head angle created greater biases for target away from the body (90°) compared with the target toward the body (270°).

Determining how stochastic noise in RFTs modulates multisensory weights was one of the goals of this experiment. In Figs. 6 and 7, we fitted Sober and Sabes' (2003) model to the data and demonstrated that both HR and NL modulate multisensory integration weights. Similar to Burns and Blohm (2010), we were able to retrieve multisensory integration weights from the covariance matrices. As has been demonstrated in Fig. A3, RFTs dramatically change the distribution of the transformed signal and consequently the covariance matrix (Alikhanian et al. 2015). To account for such variations, we calculated the determinant of the covariance matrix for calculating the multisensory weights. Figure A4 shows visual weights in both visual (*A*) and proprioceptive (*B*) coordinates.

Visual weights were lowest for head straight and no load condition in visual coordinates and increased by HR and/or applying NL. Our paired *t*-test showed that this increase was significant for all HR and NL conditions [$t(8) < -3$, $P < 0.05$]. More specifically, applying the NL increased the visual weights in visual coordinates while the head was upright [$t(8) < -3$, $P < 0.05$], whereas it did not significantly change when the head was not upright and NL was applied [$t(8) < -1$, $P \approx 0.2$]. Applying NL or HR did not significantly change visual weights in visual coordinates except for when the head rolled 30° CW [$t(8) < -18$, $P < 0.001$] or the NL applied to the left side [$t(8) < 3$, $P < 0.05$]. Combination of HR and NL only modulated the visual weights when the head was rolled 30° CW and NL applied to either side [$|t(8)| < 4$, $P < 0.05$]. Therefore, our data and model show that both noise in RFTs and the geometry of the body can influence multisensory integration in a way that is explained through changes in reliability of transformed signal by stochastic and geometrically accurate RFT processes.

ACKNOWLEDGMENTS

We thank the participants for their time and Sean Hickman for building the pulley system.

Preprint is available at https://doi.org/10.1101/182907.

GRANTS

This work was supported by Natural Sciences and Engineering Research Council of Canada and Canada Foundation for Innovation. Additionally, P. Abedi Khoozani was supported by German Academic Exchange Service.

DISCLOSURES

No conflicts of interest, financial or otherwise, are declared by the authors.

AUTHOR CONTRIBUTIONS

P.A.K. and G.B. conceived and designed research; P.A.K. performed experiments; P.A.K. analyzed data; P.A.K. and G.B. interpreted results of experiments; P.A.K. prepared figures; P.A.K. drafted manuscript; P.A.K. and G.B. edited and revised manuscript; P.A.K. and G.B. approved final version of manuscript.

ENDNOTE

At the request of the authors, readers are herein alerted to the fact that additional materials related to this manuscript may be found at the institutional Web site of the authors, which at the time of publication they indicate is: https://github.com/Parisaabedi/NeckMuscleLoad. These materials are not a part of this manuscript and have not undergone peer review by the American Physiological Society (APS). APS and the journal editors take no responsibility for these materials, for the Web site address, or for any links to or from it.

REFERENCES

Abedi Khoozani P, Standage D, Blohm G. An approximate normalization model for multisensory integration across reference frames (Abstract). *Annual Meeting of Society for Neuroscience*. San Diego, CA, 2016.

Alberts BB, Selen LP, Bertolini G, Straumann D, Medendorp WP, Tarnutzer AA. Dissociating vestibular and somatosensory contributions to spatial orientation. *J Neurophysiol* 116: 30–40, 2016. doi:10.1152/jn.00056.2016.

Alikhanian H, de Carvalho SR, Blohm G. Quantifying effects of stochasticity in reference frame transformations on posterior distributions. *Front Comput Neurosci* 9: 82, 2015. doi:10.3389/fncom.2015.00082.

Andersen RA, Buneo CA. Intentional maps in posterior parietal cortex. *Annu Rev Neurosci* 25: 189–220, 2002. doi:10.1146/annurev.neuro.25.112701.142922.

Angelaki DE, Cullen KE. Vestibular system: the many facets of a multimodal sense. *Annu Rev Neurosci* 31: 125–150, 2008. doi:10.1146/annurev.neuro.31.060407.125555.

Armstrong B, McNair P, Taylor D. Head and neck position sense. *Sports Med* 38: 101–117, 2008. doi:10.2165/00007256-200838020-00002.

Atkins JE, Fiser J, Jacobs RA. Experience-dependent visual cue integration based on consistencies between visual and haptic percepts. *Vision Res* 41: 449–461, 2001. doi:10.1016/S0042-6989(00)00254-6.

Batista AP, Buneo CA, Snyder LH, Andersen RA. Reach plans in eye-centered coordinates. *Science* 285: 257–260, 1999. doi:10.1126/science.285.5425.257.

Bauermeister M. Differences between right versus left lateral body tilt in its effect on the visual and tactual perception of verticality. *Psychol Res* 40: 183–187, 1978.

Beck JM, Latham PE, Pouget A. Marginalization in neural circuits with divisive normalization. *J Neurosci* 31: 15310–15319, 2011. doi:10.1523/JNEUROSCI.1706-11.2011.

Binder K, Heermann DW. *Monte Carlo Simulation in Statistical Physics. An Introduction* (4th ed.). Berlin; Heidelberg, Germany; New York: Springer-Verlag, 2002. doi:10.1007/978-3-662-04685-2.

Blohm G, Crawford JD. Computations for geometrically accurate visually guided reaching in 3-D space. *J Vis* 7: 4.1–22, 2007. doi:10.1167/7.5.4.

Blohm G, Keith GP, Crawford JD. Decoding the cortical transformations for visually guided reaching in 3D space. *Cereb Cortex* 19: 1372–1393, 2009. doi:10.1093/cercor/bhn177.

Buneo CA, Jarvis MR, Batista AP, Andersen RA. Direct visuomotor transformations for reaching. *Nature* 416: 632–636, 2002. doi:10.1038/416632a.

Burns JK, Blohm G. Multi-sensory weights depend on contextual noise in reference frame transformations. *Front Hum Neurosci* 4: 221, 2010. doi:10.3389/fnhum.2010.00221.

Burns JK, Nashed JY, Blohm G. Head roll influences perceived hand position. *J Vis* 11: 3, 2011. doi:10.1167/11.9.3.

Clark JJ, Yuille AL. *Data Fusion for Sensory Information Processing Systems*. Boston, MA: Springer-Verlag, 1990. doi:10.1007/978-1-4757-2076-1.

Clemens IA, De Vrijer M, Selen LP, Van Gisbergen JA, Medendorp WP. Multisensory processing in spatial orientation: an inverse probabilistic approach. *J Neurosci* 31: 5365–5377, 2011. doi:10.1523/JNEUROSCI.6472-10.2011.

Cordo PJ, Flores-Vieira C, Verschueren SM, Inglis JT, Gurfinkel V. Position sensitivity of human muscle spindles: single afferent and population representations. *J Neurophysiol* 87: 1186–1195, 2002. doi:10.1152/jn.00393.2001.

Crawford JD, Medendorp WP, Marotta JJ. Spatial transformations for eye-hand coordination. *J Neurophysiol* 92: 10–19, 2004. doi:10.1152/jn.00117.2004.

Cullen KE. The vestibular system: multimodal integration and encoding of self-motion for motor control. *Trends Neurosci* 35: 185–196, 2012. doi:10.1016/j.tins.2011.12.001.

Ernst MO, Banks MS. Humans integrate visual and haptic information in a statistically optimal fashion. *Nature* 415: 429–433, 2002. doi:10.1038/415429a.

Ernst MO, Bülthoff HH. Merging the senses into a robust percept. *Trends Cogn Sci* 8: 162–169, 2004. doi:10.1016/j.tics.2004.02.002.

Faisal AA, Selen LP, Wolpert DM. Noise in the nervous system. *Nat Rev Neurosci* 9: 292–303, 2008. doi:10.1038/nrn2258.

Fernandez C, Goldberg JM, Abend WK. Response to static tilts of peripheral neurons innervating otolith organs of the squirrel monkey. *J Neurophysiol* 35: 978–987, 1972. doi:10.1152/jn.1972.35.6.978.

Flanders M, Tillery S, Soechting J. Early stages in a sensorimotor transformation. *Behav Brain Sci* 15: 309–320, 1992. doi:10.1017/S0140525X00068813.

Gandevia SC, McCloskey DI, Burke D. Kinaesthetic signals and muscle contraction. *Trends Neurosci* 15: 62–65, 1992. doi:10.1016/0166-2236(92)90028-7.

Goodwin GM, McCloskey DI, Matthews PB. The contribution of muscle afferents to kinaesthesia shown by vibration induced illusions of movement and by the effects of paralysing joint afferents. *Brain* 95: 705–748, 1972. doi:10.1093/brain/95.4.705.

Henriques DY, Crawford JD. Role of eye, head, and shoulder geometry in the planning of accurate arm movements. *J Neurophysiol* 87: 1677–1685, 2002. doi:10.1152/jn.00509.2001.

Henriques DY, Medendorp WP, Gielen CC, Crawford JD. Geometric computations underlying eye-hand coordination: orientations of the two eyes and the head. *Exp Brain Res* 152: 70–78, 2003. doi:10.1007/s00221-003-1523-4.

Jacobson M, Matthews P. Generating uniformly distributed random Latin squares. *J Comb Des* 4: 405–437, 1996. doi:10.1002/(SICI)1520-6610(1996)4:6<405::AID-JCD3>3.0.CO;2-J.

Jones LA. Peripheral mechanisms of touch and proprioception. *Can J Physiol Pharmacol* 72: 484–487, 1994. doi:10.1139/y94-071.

Kersten D, Mamassian P, Yuille A. Object perception as Bayesian inference. *Annu Rev Psychol* 55: 271–304, 2004. doi:10.1146/annurev.psych.55.090902.142005.

Knill DC, Pouget A. The Bayesian brain: the role of uncertainty in neural coding and computation. *Trends Neurosci* 27: 712–719, 2004. doi:10.1016/j.tins.2004.10.007.

Knudsen EI, du Lac S, Esterly SD. Computational maps in the brain. *Annu Rev Neurosci* 10: 41–65, 1987. doi:10.1146/annurev.ne.10.030187.000353.

Körding KP, Beierholm U, Ma WJ, Quartz S, Tenenbaum JB, Shams L. Causal inference in multisensory perception. *PLoS One* 2: e943, 2007. doi:10.1371/journal.pone.0000943.

Körding KP, Wolpert DM. Bayesian decision theory in sensorimotor control. *Trends Cogn Sci* 10: 319–326, 2006. doi:10.1016/j.tics.2006.05.003.

Landy MS, Kojima H. Ideal cue combination for localizing texture-defined edges. *J Opt Soc Am A Opt Image Sci Vis* 18: 2307–2320, 2001. doi:10.1364/JOSAA.18.002307.

Landy MS, Maloney LT, Johnston EB, Young M. Measurement and modeling of depth cue combination: in defense of weak fusion. *Vision Res* 35: 389–412, 1995.

Lechner-Steinleitner S. Interaction of labyrinthine and somatoreceptor inputs as determinants of the subjective vertical. *Psychol Res* 40: 65–76, 1978. doi:10.1007/BF00308464.

Linkenauger SA, Witt JK, Bakdash JZ, Stefanucci JK, Proffitt DR. Asymmetrical body perception: a possible role for neural body representations. *Psychol Sci* 20: 1373–1380, 2009a. doi:10.1111/j.1467-9280.2009.02447.x.

Linkenauger SA, Witt JK, Stefanucci JK, Bakdash JZ, Proffitt DR. The effects of handedness and reachability on perceived distance. *J Exp Psychol Hum Percept Perform* 35: 1649–1660, 2009b. doi:10.1037/a0016875.

Ma WJ, Beck JM, Latham PE, Pouget A. Bayesian inference with probabilistic population codes. *Nat Neurosci* 9: 1432–1438, 2006. doi:10.1038/nn1790.

Medina J, Jax SA, Brown MJ, Coslett HB. Contributions of efference copy to limb localization: evidence from deafferentation. *Brain Res* 1355: 104–111, 2010. doi:10.1016/j.brainres.2010.07.063.

Mergner T, Huber W, Becker W. Vestibular-neck interaction and transformation of sensory coordinates. *J Vestib Res* 7: 347–367, 1997. doi:10.1016/S0957-4271(96)00176-0.

Mergner T, Nardi GL, Becker W, Deecke L. The role of canal-neck interaction for the perception of horizontal trunk and head rotation. *Exp Brain Res* 49: 198–208, 1983. doi:10.1007/BF00238580.

Mergner T, Siebold C, Schweigart G, Becker W. Human perception of horizontal trunk and head rotation in space during vestibular and neck stimulation. *Exp Brain Res* 85: 389–404, 1991. doi:10.1007/BF00229416.

Mikula L, Gaveau V, Pisella L, Khan ZA, Blohm G, Learned rather than online relative weighting of visual-proprioceptive sensory cues. *J Neurophysiol* 119: 1981–1992, 2018. doi:10.1152/jn.00338.2017.

Pitkow X, Angelaki D. How the brain might work: statistics flowing in redundant population codes (Preprint). *arXiv* arXiv:1702.03492v2 [q-bio.NC], 2017.

Press SJ. *Bayesian Statistics: Principles, Models and Applications*. New York: Wiley, 1990.

Proske U, Gandevia SC. The proprioceptive senses: their roles in signaling body shape, body position and movement, and muscle force. *Physiol Rev* 92: 1651–1697, 2012. doi:10.1152/physrev.00048.2011.

Sadeghi SG, Chacron MJ, Taylor MC, Cullen KE. Neural variability, detection thresholds, and information transmission in the vestibular system. *J Neurosci* 27: 771–781, 2007. doi:10.1523/JNEUROSCI.4690-06.2007.

Schlicht EJ, Schrater PR. Impact of coordinate transformation uncertainty on human sensorimotor control. *J Neurophysiol* 97: 4203–4214, 2007. doi:10.1152/jn.00160.2007.

Scott SH, Loeb GE. The computation of position sense from spindles in mono- and multiarticular muscles. *J Neurosci* 14: 7529–7540, 1994. doi:10.1523/JNEUROSCI.14-12-07529.1994.

Sober SJ, Körding KP. What silly postures tell us about the brain. *Front Neurosci* 6: 154, 2012. doi:10.3389/fnins.2012.00154.

Sober SJ, Sabes PN. Flexible strategies for sensory integration during motor planning. *Nat Neurosci* 8: 490–497, 2005. doi:10.1038/nn1427.

Sober SJ, Sabes PN. Multisensory integration during motor planning. *J Neurosci* 23: 6982–6992, 2003. doi:10.1523/JNEUROSCI.23-18-06982.2003.

Soechting JF, Flanders M. Moving in three-dimensional space: frames of reference, vectors, and coordinate systems. *Annu Rev Neurosci* 15: 167–191, 1992. doi:10.1146/annurev.ne.15.030192.001123.

Stein BE, Meredith MA. *The Merging of the Senses*. Cambridge, MA: MIT Press, 1993.

Stein BE, Stanford TR. Multisensory integration: current issues from the perspective of the single neuron. *Nat Rev Neurosci* 9: 255–266, 2008. [Erratum in *Nat Rev Neurosci* 9: 406, 2008.] doi:10.1038/nrn2331.

Tsay A, Savage G, Allen TJ, Proske U. Limb position sense, proprioceptive drift and muscle thixotropy at the human elbow joint. *J Physiol* 592: 2679–2694, 2014. doi:10.1113/jphysiol.2013.269365.

van Beers RJ, Sittig AC, Gon JJ. Integration of proprioceptive and visual position-information: an experimentally supported model. *J Neurophysiol* 81: 1355–1364, 1999. doi:10.1152/jn.1999.81.3.1355.

Van Beuzekom AD, Van Gisbergen JA. Properties of the internal representation of gravity inferred from spatial-direction and body-tilt estimates. *J Neurophysiol* 84: 11–27, 2000. doi:10.1152/jn.2000.84.1.11.

Vetter P, Goodbody SJ, Wolpert DM. Evidence for an eye-centered spherical representation of the visuomotor map. *J Neurophysiol* 81: 935–939, 1999. doi:10.1152/jn.1999.81.2.935.

Vingerhoets RA, De Vrijer M, Van Gisbergen JA, Medendorp WP. Fusion of visual and vestibular tilt cues in the perception of visual vertical. *J Neurophysiol* 101: 1321–1333, 2009. doi:10.1152/jn.90725.2008.

Wade SW, Curthoys IS. The effect of ocular torsional position on perception of the roll-tilt of visual stimuli. *Vision Res* 37: 1071–1078, 1997. doi:10.1016/S0042-6989(96)00252-0.

Williams J. A confidence interval for variance components. *Biometrika* 49: 278–281, 1962.